ChemPubSoc Europe

DOI: 10.1002/chem.201405482

CHEMISTRY
A European Journal
Full Paper

Diazaporphyrins

Optical, Electrochemical, and Magnetic Properties of Pyrrole- and Thiophene-Bridged 5,15-Diazaporphyrin Dimers

Satoshi Omomo,[b] Yasuhisa Maruyama,[a] Ko Furukawa,*[c] Taniyuki Furuyama,[d] Haruyuki Nakano,[e] Nagao Kobayashi,*[d] and Yoshihiro Matano*[a]

Abstract: The first examples of pyrrole- and thiophene-bridged 5,15-diazaporphyrin (DAP) dimers are prepared through Stille coupling reactions of nickel(II) and copper(II) complexes of 3-bromo-10,20-dimesityl-5,15-diazaporphyrin (mesityl = 2,4,6-trimethylphenyl) with the respective 2,5-bis-(tributylstannyl)heteroles. The effects of the heterole spacers and *meso* nitrogen atoms on the optical, electrochemical, and magnetic properties of the DAP dimers are investigated by UV/Vis absorption spectroscopy, density functional theory calculations, magnetic circular dichroism spectroscopy, cyclic voltammetry, and EPR spectroscopy. The heterole spacers are found to have a significant impact on the electronic transitions over the entire π-system. In particular, the pyrrole-bridged DAP dimers exhibit high light-harvesting potential in the low-energy visible/near-infrared region owing to the intrinsic charge-transfer character of the lowest excitation.

Introduction

Covalently linked porphyrin dimers (diporphyrins) have received considerable attention as artificial models for the special pair of chlorophylls in bacterial photosynthetic reaction centers. Furthermore, diporphyrins have been developed as a new class of optoelectronic materials, singlet oxygen sensitizers, and imaging agents.[1] A clear understanding of the effect that the spacers in such diporphyrin units have on the optical, electrochemical, and magnetic properties of the diporphyrin π-systems is essential for the design of efficient models and materials. Many studies have already been performed on this topic. For example, Osuka and Maruyama revealed that the exciton coupling of a series of naphthalene-bridged diporphyrins is related to their inter-chromophore distance and the orientation of the two porphyrin rings.[2] Several research groups have studied independently the fundamental properties of diporphyrins bridged by spacers that increase the π-conjugation, such as acetylene,[3] butadiyne,[4] pyrrole,[5] thiophene,[6,7] and oligothiophenes.[6b,8] These studies have described the electronic interactions between the two porphyrin units in both the ground and excited states. The photophysical and electrochemical behaviors of the covalently linked diporphyrins vary greatly depending on the electronic and steric effects of the intervening spacers, owing to changes in 1) the energy levels of the HOMOs and LUMOs and 2) the dihedral twist between the porphyrin rings.

5,15-Diazaporphyrin (DAP) contains an intrinsic D_{2h}-symmetric π-system with a nondegenerate HOMO/HOMO−1 and LUMO/LUMO+1. This gives rise to an intense HOMO-to-LUMO electronic transition compared with a porphyrin.[9] Therefore, DAP π-systems are promising platforms for the development of a new class of azaporphyrin-based optoelectronic materials with high light-harvesting potential in the visible/near-infrared (vis/NIR) region. To our knowledge, however, this aspect of DAP has not been addressed fully because of the lack of suitable candidates with excitation energies of less than 2 eV. Recently, we reported three types of covalently linked DAP dimers (bisDAPs)[10] and their monomer reference compounds.[11,12] In sharp contrast to their porphyrin counterparts,[13] β-β directly linked bisDAPs possess coplanar geometries and narrow HOMO–LUMO gaps (1.85–1.86 eV) compared with acetylene- and butadiyne-bridged bisDAPs (1.92–1.96 eV). These spectral features have been rationalized as being attributable to the cooperative electronic and steric effects of the *meso* nitrogen atoms of the DAP ring. Moreover, the directly linked bisDAPs have shown efficient electron-spin communication between the two DAP π-systems. Encouraged by these

[a] *Y. Maruyama, Prof. Dr. Y. Matano*
Department of Chemistry, Faculty of Science
Niigata University, Nishi-ku, Niigata 950-2181 (Japan)
Fax: (+81) 25-262-7734
E-mail: matano@chem.sc.niigata-u.ac.jp

[b] *S. Omomo*
Department of Fundamental Sciences
Graduate School of Science and Technology
Niigata University, Nishi-ku, Niigata 950-2181 (Japan)

[c] *Prof. Dr. K. Furukawa*
Center for Instrumental Analysis, Institute for Research Promotion
Niigata University, Nishi-ku, Niigata 950-2181 (Japan)
E-mail: kou-f@chem.sc.niigata-u.ac.jp

[d] *Dr. T. Furuyama, Prof. Dr. N. Kobayashi*
Department of Chemistry, Graduate School of Science
Tohoku University, Aoba-ku, Sendai 980-8578 (Japan)
E-mail: nagaok@m.tohoku.ac.jp

[e] *Prof. Dr. H. Nakano*
Department of Chemistry, Graduate School of Sciences
Kyushu University, Fukuoka 812-8581 (Japan)

Supporting information for this article is available on the WWW under http://dx.doi.org/10.1002/chem.201405482.

findings, we aimed to investigate the effects of other spacers that would increase π-conjugation on the fundamental properties of entire bisDAP π-systems. In particular, we focused on pyrrole and thiophene as the spacers, because they are electron-rich and polarizable. Herein, we report the first examples of pyrrole- and thiophene-bridged bisDAPs with coordinated nickel(II) or copper(II). These compounds were obtainable from the respective 3-bromo-DAPs and 2,5-bis(tributylstannyl)heteroles through Stille coupling reactions. The effects of the heterole spacers and *meso* nitrogen atoms on the optical, electrochemical, and magnetic properties of newly prepared bisDAPs are discussed herein.

Results and Discussion

Scheme 1 shows the synthesis of pyrrole-bridged bisMDAPs **3M** and thiophene-bridged bisMDAPs **4M** (M = Ni, Cu). 3-

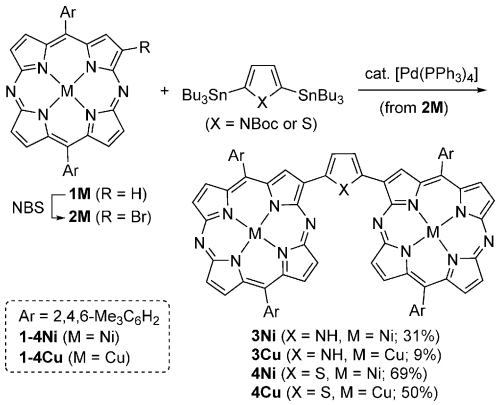

Scheme 1. Synthesis of **3M** and **4M** (M = Ni, Cu).

Bromo-NiDAP **2Ni** was obtained from β-unsubstituted 10,20-dimesityl-NiDAP **1Ni**[11] (mesityl = 2,4,6-trimethylphenyl) and *N*-bromosuccinimide (NBS) according to the reported procedure.[10] Reactions of **2Ni** with *N*-Boc-2,5-bis(tributylstannyl)pyrrole (Boc = *tert*-butoxycarbonyl) and 2,5-bis(tributylstannyl)thiophene in the presence of a catalytic amount of $Pd(PPh_3)_4$ in DMF at 120 °C afforded pyrrole-bridged bisNiDAP **3Ni** and thiophene-bridged bisNiDAP **4Ni**, respectively. During the synthesis of **3Ni**, the Boc protection was lost under the reaction conditions employed. Stille coupling reactions between **2Cu** and 2,5-bis(tributylstannyl)heteroles were also effective for the synthesis of the corresponding copper(II) complexes, **3Cu** and **4Cu**.

The heterole-bridged bisDAPs **3M** and **4M** were characterized fully by ^{1}H NMR spectroscopy (for the nickel complexes) and high-resolution mass spectrometry. In the ^{1}H NMR spectra of **3Ni** and **4Ni** in $CDCl_3$, only one set of NiDAP-derived protons was observed (Figure 1), indicating that **3Ni** and **4Ni** have C_2 or C_s symmetry on average. The ring protons of the heterole spacers (H_c) appeared as singlet peaks at δ = 7.57 ppm for **3Ni** and 8.81 ppm for **4Ni**, and peripheral protons bound to the 2 (2′) and 7 (7′) carbons (H_a and H_b) of the

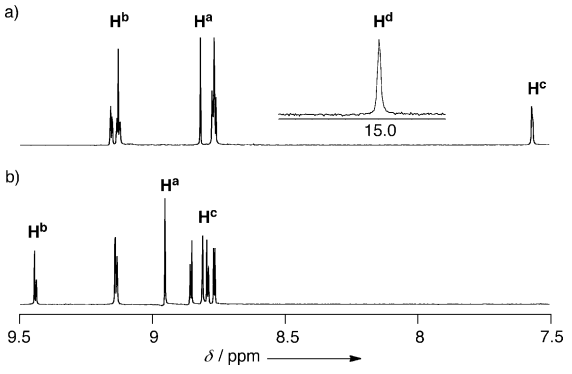

Figure 1. ^{1}H NMR spectra (δ = 7.5–9.5 ppm) of a) **3Ni** and b) **4Ni** in $CDCl_3$. The assignments of H^a–H^d protons are shown in Figure 2.

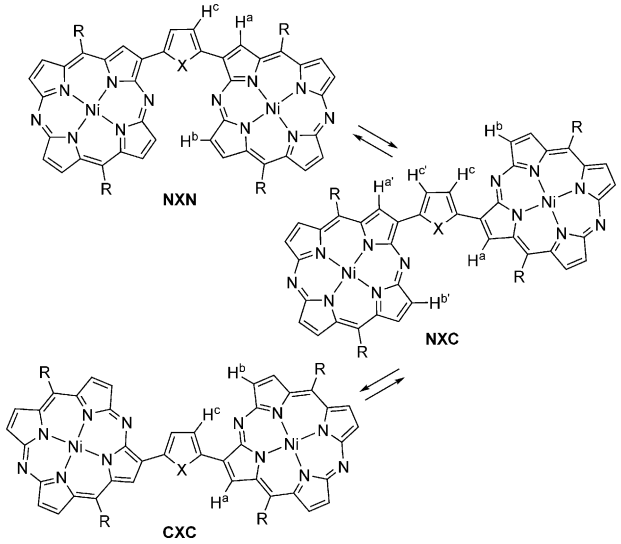

Figure 2. Possible conformations of **3Ni** (**3Ni-m**) and **4Ni** (**4Ni-m**). R = 2,4,6-$Me_3C_6H_2$ (for **3Ni** and **4Ni**) or H (for **3Ni-m** and **4Ni-m**).

DAP rings were observed at δ = 8.83 and 9.16 ppm, respectively, for **3Ni** and δ = 8.95 and 9.44 ppm, respectively, for **4Ni** (for the numbering of these protons, see Figure 2). The low-field shifts of the H_a, H_b, and H_c peaks of **4Ni** relative to the corresponding protons of **3Ni** may be caused by the difference in ring-current effects between these two dimers (see below). It is worth noting that the N–H proton (H_d) of **3Ni** is strongly deshielded (δ = 14.96 ppm) (Figure 1a). This is attributed to a hydrogen-bonding interaction between the N–H proton and the two neighboring *meso* nitrogen atoms of the DAP rings.[14] Attempts to grow high-quality single crystals of **3M** and **4M** suitable for X-ray crystallography have so far been unsuccessful.

To obtain further insight into the effects of the heterole spacers on the structures of **3Ni** and **4Ni** in solution, we conducted density functional theory (DFT) calculations with the solvent effect (PCM, CH_2Cl_2) at the B3LYP/6-311G(d,p) level (henceforth, PCM-B3LYP/6-311G(d,p)) on two models, **3Ni-m** and **4Ni-m**, in which the mesityl groups were replaced by hydrogen atoms (for details, see Supporting Information). As shown in Figure 2, there are three possible conformations,

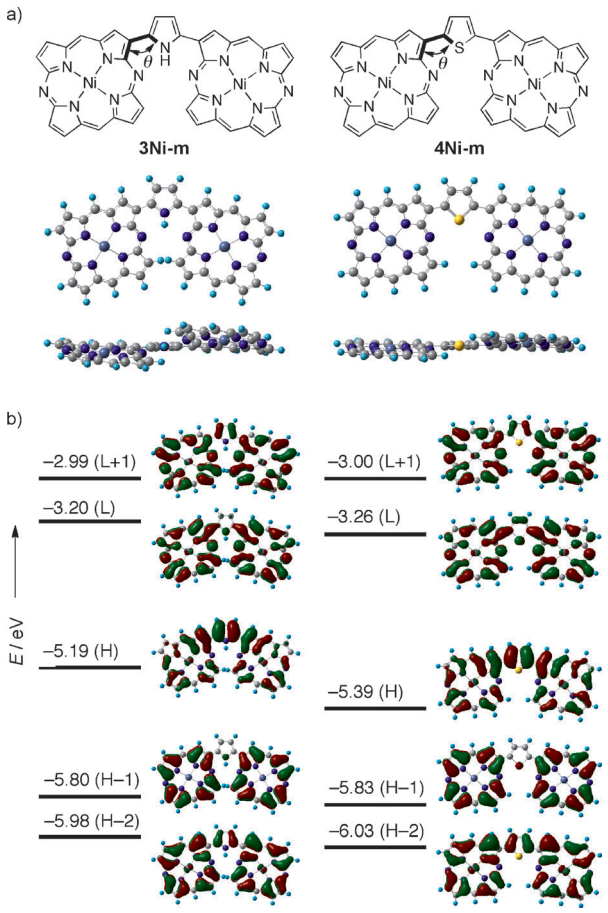

Figure 3. a) Top and front views of the optimized structures and b) selected Kohn–Sham molecular orbitals and their energies of **3 Ni-m** (left) and **4 Ni-m** (right) calculated with PCM and the DFT method. H: HOMO, L: LUMO, θ: torsion angle between the DAP and heterole rings.

which are denoted as **NXN**, **NXC**, and **CXC** (**3 Ni-m**: X = NH; **4 Ni-m**: X = S) according to the relative orientation of the heterole spacer and the two DAP rings.

The optimized structures of these models are shown in Figure 3 and Figures S1 and S2 in the Supporting Information. In each model, the **NXN** conformation is the global energy minimum, and the **NXC** and **CXC** conformations are local energy minima. In **3 Ni-m**, **N(NH)N** is more stable than **N(NH)C** and **C(NH)C** by 1.4 and 5.2 kcal mol^{-1}, respectively. The relative stability of **N(NH)N** probably stems from the cooperative hydrogen-bonding interaction between the *meso* nitrogen atoms and the pyrrolic N–H group, as seen in the ^{1}H NMR spectrum of **3 Ni**. Indeed, the theoretically calculated NMR chemical shift of the N–H proton of the **N(NH)N** conformation (δ = 14.97 ppm vs. tetramethylsilane, calculated at the PCM-B3LYP/6-311G(d,p) level) is more deshielded than that of the **C(NH)C** conformation (δ = 10.21 ppm), and is in good agreement with the observed value (δ = 14.96 ppm). These data suggest that **N(NH)N** is the dominant conformation of **3 Ni** in solution. In **4 Ni-m**, **NSN** is more stable than **NSC** and **CSC**, but their energy differences are negligibly small (0.3–0.9 kcal mol^{-1}). Additionally, the calculated rotation-energy barriers between **NSN** and **NSC** are less than 5 kcal mol^{-1} (Table S2, Supporting Information). These data indicate that three conformations of **4 Ni** may interconvert rapidly in solution. In the following discussion of the structures, orbital energies, and electronic transition energies of **3 Ni-m** and **4 Ni-m**, we will consider only the optimized structures, namely the **NXN** conformations.

As shown in Figure 3 a, **NXN** conformations have C_2 symmetry, in which the DAP rings are twisted relative to the central heterole plane owing to the steric repulsion between the two peripheral protons bound to the 7 and 7′ carbons (H^b and H$^{b'}$ in Figure 2). The calculated torsion angle around the inter-ring bond of **3 Ni-m** (θ = 12.0°; θ as defined in Figure 3 a) is appreciably larger than that of **4 Ni-m** (θ = 9.6°). Accordingly, the π conjugation between the pyrrole (spacer) and DAP rings of **3 Ni-m** may be less efficient than that between the thiophene and DAP rings of **4 Ni-m**, from a geometric point of view. It is likely that the differences in the coplanarity, distance, and orientation of the two DAP planes between **3 Ni** and **4 Ni** produce the different ring-current effects on the H^a, H^b, and H^c protons seen in the ^{1}H NMR spectra (see above).

The optical properties of the heterole-bridged bisDAPs were examined using UV/Vis/NIR absorption spectroscopy. Table 1 summarizes the absorption maxima (λ_{max}) of **1 M**, **3 M**, and **4 M** in CH_2Cl_2. As shown in Figure 4, the Soret bands of **3 Ni** and **4 Ni** are broadened and redshifted compared with those of **1 Ni**, which may be attributed to the exciton coupling between the two DAP chromophores in the heterole-bridged bisNiDAPs. Two characteristic absorption bands were observed for **3 Ni** and **4 Ni** at wavelengths longer than 500 nm. The relatively

Table 1. Optical and electrochemical data for DAPs.[a]

DAP	λ_{max} [nm][b]	E_{ox} [V][c]	E_{red} [V][c]	ΔE [V][d]
1 Ni[e]	571	+0.80	−1.40, −2.02	2.20
1 Cu[e]	577	+0.77	−1.37, −1.95	2.14
3 Ni	575, 772	+0.34, +0.70	−1.27, −1.34, −1.80 (2e)	1.61
3 Cu	587, 772	+0.29, +0.66	−1.29, −1.36, −1.82 (2e)	1.58
4 Ni	583, 687	+0.52, +0.71	−1.29, −1.35, −1.90 (2e)	1.81
4 Cu	589, 683	+0.54, +0.72	−1.28 (2e), −1.83 (2e)	1.81

[a] Measured in CH_2Cl_2. [b] Absorption maxima in the range >500 nm. [c] Oxidation (E_{ox}) and reduction (E_{red}) potentials vs. Fc/Fc$^+$, determined by DPV. Each step is a reversible 1e redox process unless otherwise noted. [d] $\Delta E = E_{ox,1} - E_{red,1}$. [e] Data from Ref. [11].

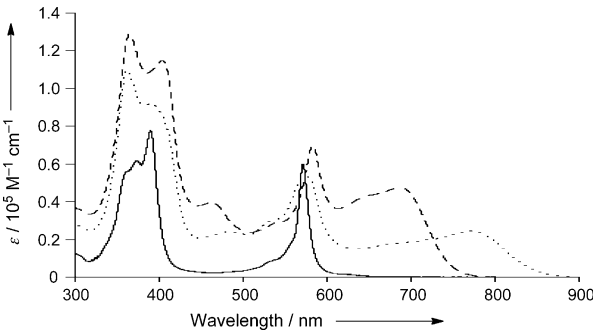

Figure 4. UV/Vis/NIR absorption spectra of **1 Ni** (solid line), **3 Ni** (dotted line), and **4 Ni** (dashed line) in CH_2Cl_2.

sharp absorption bands at $\lambda_{max}=575$ nm for **3 Ni** and 583 nm for **4 Ni** can be attributed to typical Q bands derived from the DAP chromophores, which are redshifted from the Q band of **1 Ni** ($\lambda_{max}=571$ nm). The observation that **4 Ni** displays a larger redshift ($\Delta\nu_Q=360\ cm^{-1}$) than **3 Ni** ($\Delta\nu_Q=120\ cm^{-1}$) indicates that the extension of the DAP π-system is more effective in **4 Ni** than in **3 Ni** (see above). The other characteristic bands at $\lambda_{max}=772$ nm for **3 Ni** and 687 nm for **4 Ni** are considerably broadened, and their onset wavelengths extend into the NIR region ($\lambda_{onset}=880$ nm for **3 Ni** and 780 nm for **4 Ni**). This kind of broad absorption was not observed for β–β directly linked (**5 Ni** in Figure 5), acetylene-linked, or butadiyne-linked bisNi-

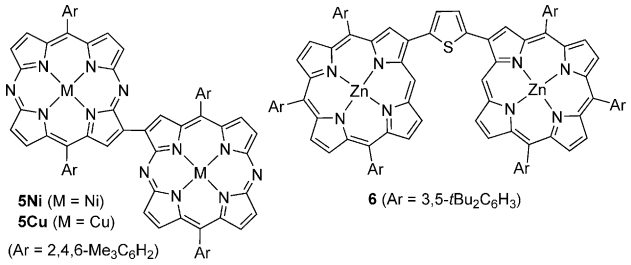

Figure 5. β–β directly linked bisDAPs, **5 Ni** and **5 Cu**, and Osuka's thiophene-bridged diporphyrin **6**.

DAPs.[10] Therefore, it appears that the heterole spacers exert a significant influence on the nature of the electronic transitions of the bisDAP π-system. Overall, the spectral features of **3 Cu** and **4 Cu** in CH_2Cl_2 are similar to those of **3 Ni** and **4 Ni**, respectively (Figure S3 in the Supporting Information).

To rationalize the observed spectral features, we performed time-dependent DFT (TD-DFT) calculations on the optimized structures of **3 Ni-m** (**N(NH)N**) and **4 Ni-m** (**NSN**). The selected excitation energies, oscillator strengths, and their assignments are summarized in Table 2 and Figure S4 in the Supporting Information. The theoretically calculated results qualitatively support the observation of two intense π–π* excitations ($f>0.2$) at energies lower than 2.5 eV together with several weak excitations. It has been found that the lowest-energy excitations for both dimers (1.62 eV for **3 Ni-m** and 1.77 eV for **4 Ni-m**) are comprised mostly of a HOMO-to-LUMO transition. As shown in Figure 3 b, in each model, the HOMO has large orbital coefficients from the central heterole ring, whereas the LUMO is rather localized on the two DAP rings. Clearly, the HOMO has a significant contribution from the heterole spacer, whereas the LUMO does not. As a result, the pyrrole-centered HOMO of **3 Ni-m** is more electron-rich and destabilized than the thiophene-centered HOMO of **4 Ni-m** (by 0.19 eV). However, the difference in the LUMO energies between **3 Ni-m** and **4 Ni-m** is small. Overall, the HOMO-to-LUMO excitation energy of **3 Ni-m** is smaller than that of **4 Ni-m**, which agrees with the observed difference seen in the lowest-energy bands of **3 Ni** and **4 Ni**.

It should be noted here that Osuka's thiophene-bridged diporphyrin **6** (Figure 5) showed a Q band at $\lambda_Q=593$ nm in its absorption spectrum in CH_2Cl_2.[7] However, no broad absorptions were detected for **6** in the longer-wavelength region (>620 nm). This difference in the optical properties of **4 Ni** and **6** may stem from the different HOMO and LUMO energies of the porphyrin and DAP chromophores; the HOMO and LUMO of **1 Ni** are lower than those of a reference porphyrin, 5,15-dimesithylporphyrinatonickel(II).[11] The theoretically calculated excitations at 2.36 eV ($f=0.293$) for **3 Ni-m** and 2.30 eV ($f=0.208$) for **4 Ni-m** correspond to the Q-type transitions observed at $\lambda_{max}=575$ nm for **3 Ni** and 583 nm for **4 Ni**, respectively. These are attributed to DAP-centered π–π* transitions.

To obtain a deeper insight into the origin of the lower-energy absorption bands (>500 nm), we performed magnetic circular dichroism (MCD) measurements of **1 Ni**, **3 Ni**, and **4 Ni** in CH_2Cl_2 (Figure 6). MCD spectroscopy provides valuable information on the ground- and excited-state degeneracy of macrocyclic π-conjugation systems, and has been used to understand the electronic structure–spectra correlations of a variety of porphyrin chromophores. The MCD intensity is associated with changes in the orbital angular momenta between ground and excited states, so the intensities of the signals for the Q bands of aromatic porphyrinoids should be large.[15] The MCD spectra of some 2,3,7,8,12,13,17,18-octaalkyldiazaporphyrins[9] and tetrabenzodiazaporphyrins[16] have been measured and discussed in detail. Owing to the absence of a threefold or

Table 2. Excitation energies and oscillator strengths of **3 Ni-m** (**N(NH)N**) and **4 Ni-m** (**NSN**) calculated with the TD-DFT method.[a]

State[b]	Excitation energy [eV/nm]	Oscillator strength (*f*)	Excitation[c]	Weight [%]
3 Ni-m				
1	1.62/763	0.524	HOMO → LUMO	98.9
2	1.87/662	0.092	HOMO → LUMO+1	87.3
9	2.11/587	0.100	HOMO → LUMO+2	89.3
11	2.36/526	0.293	HOMO−2 → LUMO	88.2
13	2.51/495	0.150	HOMO−1 → LUMO+1	76.4
24	2.85/435	0.233	HOMO−10 → LUMO	37.8
31	3.05/407	0.113	HOMO−4 → LUMO+1	42.6
40	3.28/378	1.033	HOMO → LUMO+6	48.9
4 Ni-m				
1	1.77/702	0.674	HOMO → LUMO	97.6
6	2.05/604	0.058	HOMO → LUMO+1	84.4
9	2.27/547	0.077	HOMO → LUMO+2	74.4
10	2.30/541	0.208	HOMO−1 → LUMO	44.7
			HOMO → LUMO+3	37.8
11	2.36/525	0.149	HOMO → LUMO+3	44.9
			HOMO−1 → LUMO	40.8
24	2.86/434	0.339	HOMO−10 → LUMO	38.7
29	3.04/409	0.143	HOMO−4 → LUMO	44.4
			HOMO−3 → LUMO+1	27.6
38	3.26/380	1.163	HOMO → LUMO+6	52.4

[a] TD-B3LYP/6-311G(d,p)//B3LYP/6-311G(d,p) with the solvent effect (PCM, CH_2Cl_2). [b] The states with excitation energies more than 3.3 eV or oscillator strengths less than 0.1 are not included except for the low-energy bands (<2.3 eV). [c] The excitations with weights less than 20% are not listed.

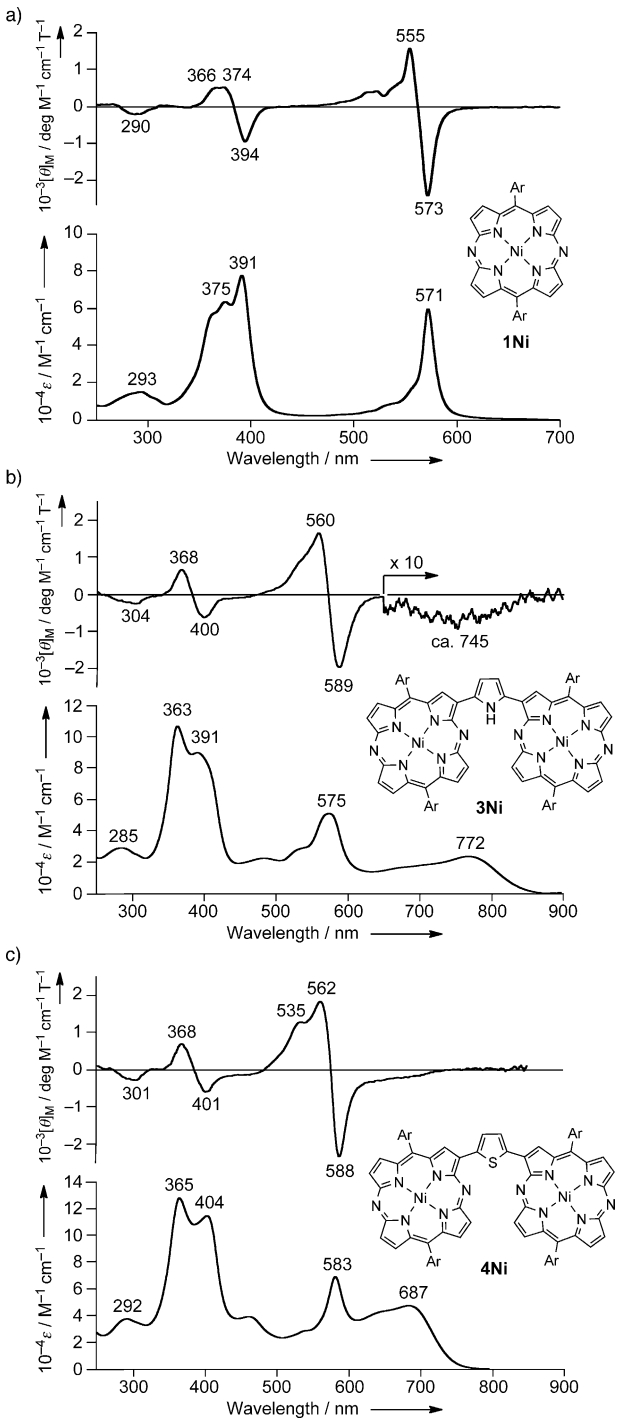

Figure 6. UV/Vis absorption (lower) and MCD (upper) spectra of a) **1 Ni**, b) **3 Ni**, and c) **4 Ni** in CH_2Cl_2. Ar = 2,4,6-$Me_3C_6H_2$.

higher symmetry axis, the MCD signals of the D_{2h}-symmetric **1 Ni** were interpreted as the superimposition of close-lying Faraday *B* terms (the so-called pseudo Faraday *A* term, Figure 6a). The changes in the sign of the MCD signal patterns in the Q-band and Soret-band regions were minus-to-plus in each case on going from the longer to shorter wavelengths. This implies that the splitting between the HOMO and HOMO−1 (ΔHOMO) is larger than that between the LUMO and LUMO+1 (ΔLUMO).[17] The interpretation deduced from the MCD spectrum is consistent with the theoretical prediction for **1 Ni-m**: ΔHOMO = 0.57 eV and ΔLUMO = 0.38 eV at the B3LYP/6-311G(d,p) level.[10] The MCD spectral features observed for **1 Ni** resemble those reported for the octaalkylDAP derivatives.[9]

In the MCD spectra of bisNiDAPs **3 Ni** and **4 Ni**, the sign of the signal changes from minus (588–589 nm) to plus (560–562 nm) in the Q-band region and from minus (400–401 nm) to plus (368 nm) in the Soret-band region (Figure 6b and 6c), which is the same as the pattern observed for **1 Ni**. The MCD curves can also probably be attributed to Faraday *B* terms, suggesting that the absorption bands at $\lambda_{max} = 575$ nm for **3 Ni** and 583 nm for **4 Ni** are basically derived from Q-type π–π* transitions of the DAP chromophores. Additionally, broad and weak MCD signals were observed at 650–850 nm for **3 Ni** and at 620–750 nm for **4 Ni**, corresponding to the broad absorptions in the same regions. The appearance of these weak MCD signals implies that the changes in angular momentum of these electronic transitions must be very small. As discussed above, the TD-DFT calculations on **3 Ni-m** and **4 Ni-m** suggest that the lowest-energy excitations are composed of a transition from the heterole-centered HOMO to the DAP-centered LUMO. From the experimental (MCD) and theoretical (TD-DFT) results, it can be concluded that the broad, redshifted absorptions around 600–880 nm are charge-transfer (CT) in character, from the heterole (donor) to the DAP (acceptor) units. It is worth noting that the intensity of the broad lowest-energy MCD signal of **3 Ni** is much weaker than that of **4 Ni**. The separation between the CT band and Q band is larger in **3 Ni** than in **4 Ni**, so the CT transition at 772 nm of **3 Ni** may interact marginally with the Q band (575 nm). Indeed, the Kohn–Sham diagrams of the HOMOs of **3 Ni-m** and **4 Ni-m** (Figure 3b) show that the contribution of the bridging pyrrole ring in **3 Ni-m** is larger than that of the thiophene ring in **4 Ni-m**. This is consistent with pyrrole having a smaller ionization energy, and hence a higher electron-donating ability, than thiophene.[18]

To investigate the electrochemical properties of the heterole-bridged bisDAPs, we first measured the redox potentials of **3 M** and **4 M** in CH_2Cl_2 using cyclic voltammetry (CV) and differential pulse voltammetry (DPV) with Bu_4NPF_6 as the supporting electrolyte. The oxidation and reduction potentials (E_{ox} and E_{red}) of **1 M**, **3 M**, and **4 M** versus the ferrocene/ferrocenium couple (Fc/Fc^+) are summarized in Table 1. The pyrrole-bridged bisNiDAP **3 Ni** displayed reversible oxidation and reduction processes at +0.34/+0.70 V and −1.27/−1.34/−1.80 V, respectively, within the observable range from −2.1 to +1.0 V versus Fc/Fc^+. The thiophene-bridged bisNiDAP **4 Ni** displayed reversible oxidation and reduction processes at +0.52/+0.71 V and −1.29/−1.35/−1.90 V, respectively (Figure S5a,b in the Supporting Information). The copper complexes **3 Cu** and **4 Cu** displayed similar voltammograms (Figure S5c,d in the Supporting Information). The heterole bridges were found to enhance greatly the electron-donating ability of the entire π-system. The first oxidation potentials ($E_{ox,1}$) of **3 Ni** and **4 Ni** are more negative than that of **1 Ni** by 0.46 and 0.28 V, respectively. In contrast, the effect of the heterole spacers on the first reduction potentials ($E_{red,1}$) is fairly small. The electronic effects of the

heterole spacers on the HOMO and LUMO energies are similar to those predicted by the DFT calculations. Furthermore, electrochemical HOMO–LUMO gaps ($\Delta E = E_{ox,1} - E_{red,1}$) of **3Ni** (1.61 V) and **4Ni** (1.81 V) are in good agreement with the optical HOMO–LUMO gaps determined from the λ_{max} values of the lowest-energy transitions. The splitting of the first and second oxidation processes ($\Delta E_{ox} = E_{ox,2} - E_{ox,1}$) of **3Ni** (0.36 V) is larger than that of **4Ni** (0.19 V), reflecting the difference in the $E_{ox,1}$ values between **3Ni** and **4Ni**, whereas the $E_{red,1}$ values are similar. The large potential differences and the reversibility of the voltammograms indicate that both radical cations are stable species. However, the splitting energies of the first and second reduction processes ($\Delta E_{red} = E_{red,1} - E_{red,2}$) of **3Ni** (0.07 V) and **4Ni** (0.06 V) are smaller than that reported for **5Ni** (ΔE_{red} = 0.19 V).[10] This implies that the electronic coupling through the heterole spacers may be less effective in the π-radical anions.

To obtain insight into the optical properties of the radical cations, we performed spectroelectrochemical measurements on the chemical oxidations of **3Ni** and **4Ni** in CH_2Cl_2 with tris(4-bromophenyl)ammoniumyl hexachloroantimonate (TBAHA) as the oxidant. As shown in Figure 7, clear spectral

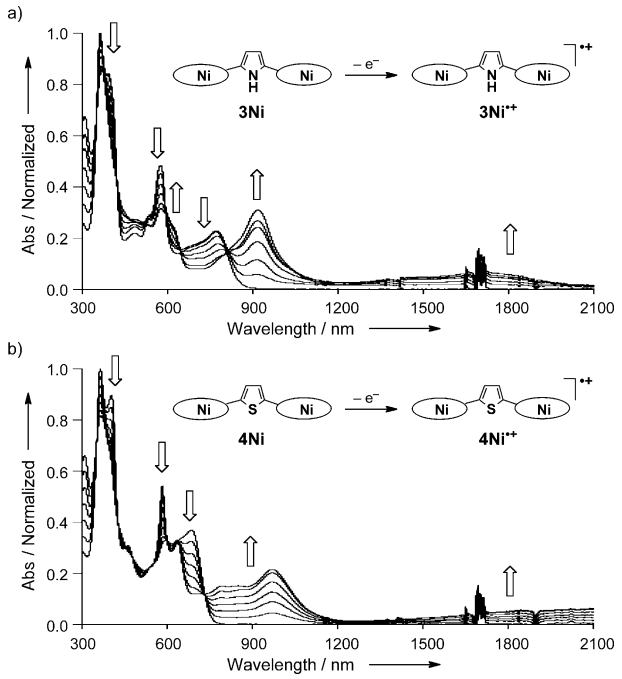

Figure 7. Spectroscopic changes observed in the oxidation processes a) from **3Ni** to its π-radical cation **3Ni**$^{+\cdot}$ and b) from **4Ni** to its π-radical cation **4Ni**$^{+\cdot}$ in CH_2Cl_2 by using TBAHA as an oxidant.

changes with several isosbestic points were observed during the course of the one-electron oxidation processes. The characteristic absorption bands attributed to the DAP-based π-radical cations appeared at 800–1150 nm (λ_{max} = 918 nm) for **3Ni**$^{\cdot+}$ and at 800–1200 nm (λ_{max} = 970 nm) for **4Ni**$^{\cdot+}$. It should be noted that very broad absorptions also appeared in the short-wavelength IR region at wavelengths greater than 1200 nm. These lower-energy broad bands have been assigned as intervalence charge-transfer bands between the heterole cation centers and the two DAP rings. The spin densities of radical cations for **3Ni-m** and **4Ni-m** were calculated using the DFT method. As shown in Figure S6 in the Supporting Information, the electron spin is delocalized, but mainly distributed around the five-membered rings in both (**3Ni-m**)$^{\cdot+}$ and (**4Ni-m**)$^{\cdot+}$. The different λ_{max} values of **3Ni**$^{\cdot+}$ and **4Ni**$^{\cdot+}$ suggest that the electron-spin communication through the thiophene spacer is more effective than through the pyrrole spacer in the radical cations of bisNiDAPs.

Finally, the effects of the heterole spacers on the exchange interaction of electron spins between the two CuDAP π-systems in **3Cu** and **4Cu** were examined using electron paramagnetic resonance (EPR) spectroscopy. The measurements were conducted in 2-methyltetrahydrofuran at 35 K, and the resulting spin Hamiltonian parameters are listed in Figure S7 in the Supporting Information. Figure 8 summarizes the EPR spectra

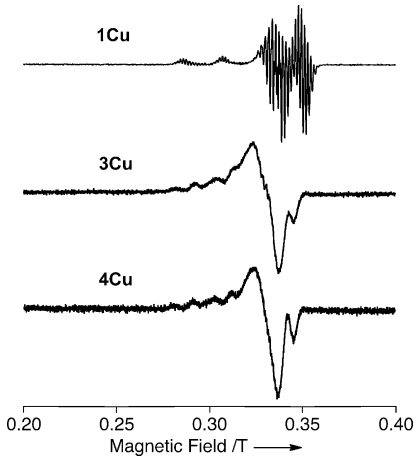

Figure 8. EPR spectra of **1Cu**, **3Cu**, and **4Cu** in toluene at 40 K (**1Cu**) or in 2-methyltetrahydrofuran at 35 K (**3Cu**, **4Cu**).

of **1Cu**, **3Cu**, and **4Cu**. As reported previously,[10] **1Cu** exhibited an EPR signal (g = 2.052–2.168) with well-resolved hyperfine structures attributed to the nuclear spins of one copper(II) and the four core nitrogen atoms (Figure 8, top). The EPR signals of the heterole-bridged bisCuDAPs **3Cu** and **4Cu** (Figure 8, middle and bottom) were well simulated as two magnetically coupled CuDAPs, in which the hyperfine splitting width for the copper nuclei in bisCuDAPs was half that of **1Cu**. These spectral features seen in **3Cu** and **4Cu** resemble those seen in **5Cu**.[10]

To compare the exchange interaction between the two copper(II) spins of **3Cu** with **4Cu**, we next measured the temperature dependence of the EPR signal intensity (I), which is proportional to the magnetic susceptibility. In both cases, the IT values decreased sharply when the temperature dropped below 10 K (Figure S8 in the Supporting Information). This IT–T behavior is characteristic of an antiferromagnetic coupling between the two copper(II) ions. Accordingly, the EPR signals observed for **3Cu** and **4Cu** are probably caused by a thermally populated triplet state (S = 1). Furthermore, the experimentally observed IT–T plots of **3Cu** and **4Cu** were fitted to the Blea-

ney–Bowers equation[19] to obtain exchange coupling constants (J/k_B in which k_B is the Boltzmann constant). The J/k_B values of −1.7 K for **3Cu** and −2.9 K for **4Cu** are smaller than that of **5Cu** ($J/k_B = -13.8$ K) and comparable to that of Osuka's *meso–meso*, β–β, β–β triply fused Cu-diporphyrin ($J/k_B = -2.06$ K).[20] Thus, it appears that the insertion of the heterole ring reduces the antiferromagnetic coupling between the two DAP units as compared with the β–β direct linkage.

The absolute J/k_B value of **4Cu** is slightly larger than that of **3Cu**, so it can also be concluded that the thiophene bridge allows more electron-spin communication between the two CuDAP units than the pyrrole bridge. This may indicate that the π conjugation through the thiophene ring is more efficient than that through the pyrrole ring in the copper complexes. On the basis of the point dipole approximation, the spin–spin distances of **3Cu** and **4Cu** were estimated to be 10.6 and 11.8 Å, respectively, from the *D* values of the spin Hamiltonian parameters. These distances are close to the Ni···Ni distances in the **NXN** conformation of **3Ni-m** (10.5 Å) and **4Ni-m** (11.8 Å) as calculated through DFT. Considering the structural similarity between NiDAP and CuDAP,[9] these results indicate that the **NXN** conformation is dominant under the EPR measurement conditions.

Conclusion

We have prepared the first examples of pyrrole- and thiophene-bridged bisDAPs **3M** and **4M** using the Stille coupling reactions of 3-bromoDAPs **2M** with the respective 2,5-bis(tributylstannyl)heteroles. Various spectroscopic and electrochemical measurements of **3M** and **4M**, as well as DFT calculations on their models, have revealed that the heterole spacers exert a critical impact on the structural, optical, electrochemical, and magnetic properties of the covalently linked bisDAP π-systems. Most importantly, both heterole spacers impart an intrinsic charge-transfer character to the lowest-energy excitations, which are observed as broad, moderately intense absorptions in the range 600–880 nm. These features were not observed for the previously reported bisDAPs, and highlight the synergistic effects of the heterole spacer and DAP π-systems. The small but distinct differences in the electronic and geometric effects between the pyrrole and thiophene spacers on the entire π-system are also noteworthy. The pyrrole spacer is more electron-donating, and thus, has a narrower HOMO–LUMO gap, whereas the thiophene spacer conjugates the adjacent DAP units more effectively. These results support the premise that heterole-bridged DAP dimers could be useful models for a new class of azaporphyrin-based optoelectronic materials with high light-harvesting potential in the Vis/NIR region. Further studies on linker effects on DAP derivatives with extended π-systems are now underway.

Experimental Section

General remarks, synthetic procedures, and the characterization data of new compounds are provided in the Supporting Information.

Computational details

The geometries of **3Ni-m** and **4Ni-m** in solution were optimized using the DFT method, in which the solvent effect of CH_2Cl_2 was included through the polarizable continuum model (PCM) method.[21] The basis sets used were the 6–311G(d,p) basis set[22] for H, C, and N, and the Wachters–Hay all-electron basis set[23] supplemented with one f-function (exponent: 1.29) for Ni. The functional of DFT was the Becke, three-parameter, Lee–Yang–Parr (B3LYP) exchange-correlation functional.[24] We confirmed that the optimized geometries were not in saddle but in stable points. The Cartesian coordinates are summarized in Table S1 (Supporting Information). The proton chemical shifts (vs. tetramethylsilane) in solution were calculated at the DFT level with gauge-including atomic orbitals (GIAOs). The excitation energies and oscillator strengths listed in Table 2 were computed using the time-dependent DFT (TD-DFT) method. The geometries of the radical cations of **3Ni-m** and **4Ni-m** in solution were also optimized, and their spin densities were computed using the DFT method with the same basis set and exchange-correlation functional as those of the neutral species. All the calculations were performed using the Gaussian 09 suite of programs.[25] Selected Kohn–Sham molecular orbitals and their energies are summarized in Figure 3b.

Magnetic circular dichroism spectroscopy measurements

Electronic absorption spectra were recorded on a JASCO V-570 spectrophotometer. Magnetic circular dichroism spectra were recorded on a JASCO J-725 spectrodichrometer equipped with a JASCO electromagnet, which produces magnetic fields of up to 1.03 T (1 T = 1 Tesla) with both parallel and antiparallel fields. The magnitudes were expressed in terms of molar ellipticity per tesla ($[\theta]_M$/deg dm^3 mol^{-1} cm^{-1} T^{-1}).

EPR measurements

A solution of **3Cu** or **4Cu** in 2-methyltetrahydrofuran (1 mL) in a sealable EPR tube was degassed by repeated freeze/pump/thaw cycles and sealed under vacuum by flame. The EPR spectra were recorded using a Bruker EMX plus spectrometer equipped with an Oxford ESR900 He-flow-type cryostat. The temperature was controlled by using an Oxford ITC503 temperature controller. Spectral simulation was performed using the EasySpin program package.[26] The simulated spectra are in good agreement with those observed at 35 K (Figure S7 in the Supporting Information).

The spin Hamiltonian for **3Cu** and **4Cu** is expressed by Equation (1), in which μ_B, μ_N, **S**, **g**, **A**, **D**, $\mathbf{B}_0$, and **I** denote the Bohr magneton, the nuclear magneton, the electron-spin operator, the *g* tensor of the electron spin, the hyperfine structure tensor, the fine structure tensor, the external magnetic field, and the nucleus spin operator, respectively.

$$H = (\mu_B \mathbf{S}_1 \cdot \mathbf{g}_1 \cdot \mathbf{B}_0 + \mu_N \mathbf{I}_{Cu1} \cdot \mathbf{g}_{n1} \cdot \mathbf{B}_0 + \mathbf{S}_1 \cdot \mathbf{A}_1 \cdot \mathbf{I}_{Cu1}) + (\mu_B \mathbf{S}_2 \cdot \mathbf{g}_2 \cdot \mathbf{B}_0 + \mu_N \mathbf{I}_{Cu2} \cdot \mathbf{g}_{n2} \cdot \mathbf{B}_0 + \mathbf{S}_2 \cdot \mathbf{A}_2 \cdot \mathbf{I}_{Cu2}) + \mathbf{S}_1 \cdot \mathbf{D}_{12} \cdot \mathbf{S}_2 \quad (1)$$

We assume that the $\mathbf{g}_2$, $\mathbf{A}_1$, $\mathbf{A}_2$, and $\mathbf{D}_{12}$ tensors are coaxial with the $\mathbf{g}_1$ tensor. The selected spin-Hamiltonian parameters are summarized in Figure S7 in the Supporting Information. We also examined the temperature dependence of the signal intensity *I* (Figure S8 in the Supporting Information), which is proportional to the magnetic susceptibility χ in the range 4 to 90 K. The observed temperature dependence of the *IT* values was fitted by the Bleaney–Bowers

equation (Eq. (2)], in which N, g, k_B, T, and J denote the Avogadro number, the mean value of the principal values of the g tensor, the Boltzmann factor, the temperature, and the exchange coupling constant, respectively.[19]

$$\chi_{spin} = \frac{2Ng^2\mu_B^2}{k_B T[3 + \exp(-J/k_B T)]} \quad (2)$$

As a result, J/k_B could be estimated as -1.7 K for **3 Cu** and -2.9 K for **4 Cu**.

Acknowledgements

This work was supported by JSPS KAKENHI Grant Numbers 25109524, 24109008, 25109502, and by the Nagase Foundation. SO and YM thank Prof. Eiji Tayama (Niigata University) for his kind support and valuable comments.

Keywords: diazaporphyrins · EPR spectroscopy · macrocyclic compounds · porphyrinoids · transition metals

[1] a) M. K. Kuimova, H. A. Collins, M. Balaz, E. Dahlstedt, J. A. Levitt, N. Sergent, K. Suhling, M. Drobizhev, N. S. Makarov, A. Rebane, H. L. Anderson, D. Phillips, *Org. Biomol. Chem.* **2009**, *7*, 889; b) M. Pawlicki, H. A. Collins, R. G. Denning, H. L. Anderson, *Angew. Chem. Int. Ed.* **2009**, *48*, 3244; *Angew. Chem.* **2009**, *121*, 3292; c) M. K. Kuimova, M. Balaz, H. L. Anderson, P. R. Ogilby, *J. Am. Chem. Soc.* **2009**, *131*, 7948; d) N. Aratani, A. Osuka in *Handbook of Porphyrin Science, Vol 1* (Eds: K. Kadish, K. M. Smith, R. Guilard), World Scientific, New Jersey, **2010**, pp. 1–132; e) Z. S. Yoon, J. Yang, H. Yoo, S. Cho, D. Kim in *Handbook of Porphyrin Science, Vol. 1* (Eds: K. Kadish, K. M. Smith, R. Guilard), World Scientific, New Jersey, **2010**, pp. 439–505, and references therein.

[2] A. Osuka, K. Maruyama, *J. Am. Chem. Soc.* **1988**, *110*, 4454.

[3] For example, see: a) V. S.-Y. Lin, S. G. DiMagno, M. J. Therien, *Science* **1994**, *264*, 1105; b) P. J. Angiolillo, V. S.-Y. Lin, J. M. Vanderkooi, M. J. Therien, *J. Am. Chem. Soc.* **1995**, *117*, 12514; c) R. Kumble, S. Palese, V. S.-Y. Lin, M. J. Therien, R. M. Hochstrasser, *J. Am. Chem. Soc.* **1998**, *120*, 11489; d) M. Drobizhev, Y. Stepanenko, Y. Dzenis, A. Karotki, A. Rebane, P. N. Taylor, H. L. Anderson, *J. Am. Chem. Soc.* **2004**, *126*, 15352; e) M. Toganoh, T. Takayama, N. Ritesh, N. Kimizuka, H. Furuta, *Chem. Lett.* **2011**, *40*, 1021.

[4] For example, see: a) D. P. Arnold, L. J. Nitschinsk, *Tetrahedron* **1992**, *48*, 8781; b) J. J. Gosper, M. Ali, *J. Chem. Soc. Chem. Commun.* **1994**, 1707; c) B. König, H. Zieg, *Synthesis* **1998**, 171; d) P. N. Taylor, A. P. Wylie, J. Huuskonen, H. L. Anderson, *Angew. Chem. Int. Ed.* **1998**, *37*, 986; *Angew. Chem.* **1998**, *110*, 1033; e) D. P. Arnold, A. Genga, D. Manno, G. Micocci, A. Serra, A. Tepore, L. Valli, *Colloids Surf. A* **2002**, *198–200*, 897; f) L.-M. Jin, L. Chen, J.-J. Yin, J.-M. Zhou, C.-C. Guo, Q.-Y. Chen, *J. Org. Chem.* **2006**, *71*, 527; g) I. Hisaki, S. Hiroto, K. S. Kim, S. B. Noh, D. Kim, H. Shinokubo, A. Osuka, *Angew. Chem. Int. Ed.* **2007**, *46*, 5125; *Angew. Chem.* **2007**, *119*, 5217; h) C. She, S. Easwaramoorthi, P. Kim, S. Hiroto, I. Hisaki, H. Shinokubo, A. Osuka, D. Kim, J. T. Hupp, *J. Phys. Chem. A* **2010**, *114*, 3384.

[5] C. Maeda, H. Shinokubo, A. Osuka, *Org. Lett.* **2010**, *12*, 1820.

[6] a) K. Fujisawa, A. Satake, S. Hirota, Y. Kobuke, *Chem. Eur. J.* **2008**, *14*, 10735; b) M. Regehly, T. Wang, U. Siggel, J. H. Fuhrhop, B. Röder, *J. Phys. Chem. B* **2009**, *113*, 2526; c) T. Umeyama, T. Takamatsu, N. Tezuka, Y. Matano, Y. Araki, T. Wada, O. Yoshikawa, T. Sagawa, S. Yoshikawa, H. Imahori, *J. Phys. Chem. C* **2009**, *113*, 10798.

[7] a) J. Song, S. Y. Jang, S. Yamaguchi, J. Sankar, S. Hiroto, N. Aratani, J.-Y. Shin, S. Easwaramoorthi, K. S. Kim, D. Kim, H. Shinokubo, A. Osuka, *Angew. Chem. Int. Ed.* **2008**, *47*, 6004; *Angew. Chem.* **2008**, *120*, 6093; b) J. Song, N. Aratani, H. Shinokubo, A. Osuka, *Chem. Sci.* **2011**, *2*, 748.

[8] a) F. Odobel, S. Suresh, E. Blart, Y. Nicolas, J.-P. Quintard, P. Janvier, J.-Y. Le Questel, B. Illien, D. Rondeau, P. Richomme, T. Häupl, S. Wallin, L. Hammarström, *Chem. Eur. J.* **2002**, *8*, 3027; b) S. Mukherjee, S. Banerjee, A. K. Bauri, S. Bhattacharya, *J. Mol. Struct.* **2011**, *1004*, 13; c) S. Wallin, L. Hammarström, E. Blart, F. Odobel, *Photochem. Photobiol. Sci.* **2006**, *5*, 828.

[9] a) N. Kobayashi in *The Porphyrin Handbook, Vol. 2* (Eds: K. Kadish, K. M. Smith, R. Guilard), Academic Press, San Diego, **2000**, pp. 301–360; b) H. Ogata, T. Fukuda, K. Nakai, Y. Fujimura, S. Neya, P. A. Stuzhin, N. Kobayashi, *Eur. J. Inorg. Chem.* **2004**, 1621; c) N. Pan, Y. Bian, M. Yokoyama, R. Li, T. Fukuda, S. Neya, J. Jiang, N. Kobayashi, *Eur. J. Inorg. Chem.* **2008**, 5519.

[10] Y. Matano, D. Fujii, T. Shibano, K. Furukawa, T. Higashino, H. Nakano, H. Imahori, *Chem. Eur. J.* **2014**, *20*, 3342.

[11] a) Y. Matano, T. Shibano, H. Nakano, H. Imahori, *Chem. Eur. J.* **2012**, *18*, 6208; b) Y. Matano, T. Shibano, H. Nakano, Y. Kimura, H. Imahori, *Inorg. Chem.* **2012**, *51*, 12879.

[12] Shinokubo and coworkers also isolated **1 Ni** in their metal-template synthesis of azacorrole. See: M. Horie, Y. Hayashi, S. Yamaguchi, H. Shinokubo, *Chem. Eur. J.* **2012**, *18*, 5919.

[13] S. Cho, M.-C. Yoon, J. M. Lim, P. Kim, N. Aratani, Y. Nakamura, T. Ikeda, A. Osuka, D. Kim, *J. Phys. Chem. B* **2009**, *113*, 10619.

[14] For the protonation on the *meso* nitrogen atoms of DAP, see: P. A. Stuzhin, *J. Porphyrins Phthalocyanines* **1999**, *3*, 500.

[15] a) M. J. Stillman, T. Nyokong in *Phthalocyanines: Properties and Applications, Vol. 1* (Eds: C. C. Leznoff, A. B. P. Lever), VCH, Weinheim, **1989**, pp. 133–289; b) J. Mack, M. J. Stillman, N. Kobayashi, *Coord. Chem. Rev.* **2007**, *251*, 429–453; c) N. Kobayashi, A. Muranaka, J. Mack, *Circular Dichroism and Magnetic Circular Dichroism Spectroscopy for Organic Chemists*, RSC, UK, **2011**.

[16] a) E. A. Makarova, V. N. Kopranenkov, V. K. Shevtsov, E. A. Lukyanets, *Chem. Heterocycl. Compd.* **1989**, *25*, 1159; b) J. Mack, L. Sosa-Vargas, S. J. Coles, G. J. Tizzard, I. Chambrier, A. N. Cammidge, M. J. Cook, N. Kobayashi, *Inorg. Chem.* **2012**, *51*, 12820.

[17] a) J. Michl, *J. Am. Chem. Soc.* **1978**, *100*, 6801; b) J. Michl, *J. Am. Chem. Soc.* **1978**, *100*, 6812; c) J. D. Keegan, A. M. Stolzenberg, Y. C. Lu, R. E. Linder, G. Barth, A. Moscowitz, E. Bunnenberg, C. Djerassi, *J. Am. Chem. Soc.* **1982**, *104*, 4305.

[18] a) T. L. Kunii, H. Kuroda, *Theor. Chim. Acta* **1968**, *11*, 97; b) F. De Proft, N. Sablon, D. J. Tozer, P. Geerlings, *Faraday Discuss.* **2007**, *135*, 151.

[19] R. L. Carlin, *Magnetochemistry*; Springer, Berlin, **1986**.

[20] T. Ikeue, K. Furukawa, H. Hata, N. Aratani, H. Shinokubo, T. Kato, A. Osuka, *Angew. Chem. Int. Ed.* **2005**, *44*, 6899; *Angew. Chem.* **2005**, *117*, 7059.

[21] M. T. Cancès, B. Mennucci, J. Tomasi, *J. Chem. Phys.* **1997**, *107*, 3032.

[22] R. Krishnan, J. S. Binkley, R. Seeger, J. A. Pople, *J. Chem. Phys.* **1980**, *72*, 650.

[23] a) A. J. H. Wachters, *J. Chem. Phys.* **1970**, *52*, 1033; b) P. J. Hay, *J. Chem. Phys.* **1977**, *66*, 4377; c) K. Raghavachari, G. W. Trucks, *J. Chem. Phys.* **1989**, *91*, 1062.

[24] a) A. D. Becke, *J. Chem. Phys.* **1993**, *98*, 5648; b) C. Lee, W. Yang, R. G. Parr, *Phys. Rev. B* **1988**, *37*, 785.

[25] Gaussian 09, Revision B.01, M. J. Frisch, G. W. Trucks, H. B. Schlegel, G. E. Scuseria, M. A. Robb, J. R. Cheeseman, G. Scalmani, V. Barone, B. Mennucci, G. A. Petersson, H. Nakatsuji, M. Caricato, X. Li, H. P. Hratchian, A. F. Izmaylov, J. Bloino, G. Zheng, J. L. Sonnenberg, M. Hada, M. Ehara, K. Toyota, R. Fukuda, J. Hasegawa, M. Ishida, T. Nakajima, Y. Honda, O. Kitao, H. Nakai, T. Vreven, J. A. Montgomery, Jr., J. E. Peralta, F. Ogliaro, M. Bearpark, J. J. Heyd, E. Brothers, K. N. Kudin, V. N. Staroverov, R. Kobayashi, J. Normand, K. Raghavachari, A. Rendell, J. C. Burant, S. S. Iyengar, J. Tomasi, M. Cossi, N. Rega, J. M. Millam, M. Klene, J. E. Knox, J. B. Cross, V. Bakken, C. Adamo, J. Jaramillo, R. Gomperts, R. E. Stratmann, O. Yazyev, A. J. Austin, R. Cammi, C. Pomelli, J. W. Ochterski, R. L. Martin, K. Morokuma, V. G. Zakrzewski, G. A. Voth, P. Salvador, J. J. Dannenberg, S. Dapprich, A. D. Daniels, Ö. Farkas, J. B. Foresman, J. V. Ortiz, J. Cioslowski, D. J. Fox, Gaussian, Inc., Wallingford CT, 2009.

[26] S. Stoll, A. Schweiger, *J. Magn. Reson.* **2006**, *178*, 42.

Received: October 1, 2014
Published online on November 27, 2014